Available online at www.sciencedirect.com
ScienceDirect
Sensors and Actuators B 117 (2006) 401–407
SENSORS AND ACTUATORS B CHEMICAL
www.elsevier.com/locate/snb

Investigation of the profile effect on the sensitivity enhancement of nanowire-mediated localized surface plasmon resonance biosensors

Kyung Min Byun [a], Donghyun Kim [b,*], Sung June Kim [a]

[a] School of Electrical Engineering and Computer Science, Seoul National University, Seoul, Republic of Korea
[b] School of Electrical and Electronic Engineering, Yonsei University, Seoul, Republic of Korea

Received 9 June 2005; accepted 18 November 2005
Available online 27 December 2005

Abstract

Localized surface plasmon resonance (SPR) biosensors with metallic nanowires regularly patterned on a gold film are considered for sensitivity enhancement. The theoretical investigation was conducted using rigorous coupled wave analysis in terms of various design metrics, such as the resonance angle shift, the SPR curve angular width, and the minimum reflectance at resonance. The results show that nanowires of a T-profile present more effective sensitivity enhancement than an inverse T-profile. The sensitivity enhancement mediated by the presence of nanowires has also been clarified qualitatively based on the dispersion relation between metal film involving nanowires and surrounding dielectric medium. The study is expected to provide extremely high sensitivity in SPR-based biosensing.

Keywords: Surface plasmon resonance; Biosensor; Nanowires; Localized surface plasmon; Rigorous coupled wave analysis

1. Introduction

Surface plasmon resonance (SPR) is widely used in optical biosensors for detection and analysis of biological and chemical interactions [1–5]. SPR is attributed to the excitation of surface plasmon polaritons (SPPs) when a TM-polarized beam of light incident on a thin conducting metal film between two dielectric media is coupled to surface plasmons formed in the film [6]. These plasmons resonantly couple with the incident light at a specific resonance angle as the momentum matching between an incident photon and a SPP is achieved. A conventional SPR biosensor is based on the attenuated total reflection configuration, in which an incident beam is coupled through a prism on a slide glass coated with a gold film, as shown in Fig. 1 [7]. As incident light passes through a transparent dielectric superstrate and is reflected at the metal film to a photodetector, a small change in refractive index induced by interactions amongst biomolecules on the metal surface results in an angular shift of resonance. By measuring the resonance shift, it is possible to quantify a surface reaction of interest. SPR-based biosensors have successfully measured various biochemical reactions such as antibody–antigen binding [8,9], DNA hybridisation [10], biomaterial and cell receptor interactions [11], and other adsorption processes [12,13].

It has been well known that use of metallic nanostructures on a SPR-biosensor leads to a large shift in resonance angles, compared to a conventional SPR biosensor, through strong optical coupling between SPPs on a metal film and localized surface plasmons (LSPs) of plasma oscillations confined in nanostructures [14,15]. When the LSP resonance condition is satisfied, the existence of nanostructures deforms the dispersion relation of SPP modes, which results in damping of SPP features [16,17]. Since LSP effects usually provide improved sensitivity, SPR biosensors that exploit nanostructures have drawn tremendous interests in recent years. It has been empirically reported that nanostructures can enhance the sensitivity of an SPR biosensor by one to two orders of magnitude [18–20].

In general, an SPR curve is obtained by varying either an incidence angle or light wavelength. While SPR sensors mainly measure the resonance angle shift, oftentimes curve angular width (CAW) and minimum reflectance at resonance (MRR) need also be taken into account for improved quantitative analysis of target analyte binding events [16,21,22]. In the presence of nanostructures, a measured SPR curve shows different

* Corresponding author. Tel.: +82 2 2123 2777; fax: +82 2 313 2879.
E-mail address: kimd@yonsei.ac.kr (D. Kim).

0925-4005/$ – see front matter © 2005 Elsevier B.V. All rights reserved.
doi:10.1016/j.snb.2005.11.038

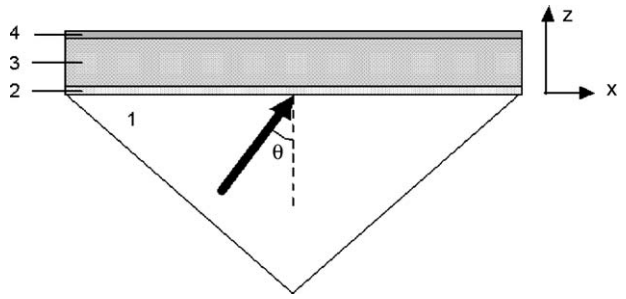

Fig. 1. Schematic diagram of a conventional SPR biosensor. The TM-polarized light in the xz-plane is incident at an angle θ. Layers 1, 2, 3, and 4 represent a BK7 glass prism, a binding film of chromium, a SPP supporting gold film, and target analytes, respectively.

resonance properties, such as increased SPR CAW and MRR as well as an additional shift in resonance angle, possibly due to absorptive damping and localized coupling [6,14,16,17,23].

In our previous study, nanowire-mediated localized SPR biosensors were found to offer significant enhancement in sensitivity, mainly induced by resonantly excited LSPs and LSP–SPP interactions [24]. More specifically, a SPR structure based on nanowires of a T-profile showed better sensitivity than those of an inverse T-profile. However, only angular shift of resonance was employed as a metric for the calculation since it was the most conveniently available, so that the structure optimized for maximum sensitivity enhancement was in fact suboptimal from functional aspects of a biosensor.

In this paper, we investigate a SPR biosensor structure, in which excitation of and interactions with LSPs are mediated by nanowires, and extend the analysis based on comprehensive design metrics, other than sensitivity enhancement induced by resonance angle shift, such as variations of MRR and SPR CAW. Optimal design parameters of nanowires are determined in terms of the sensor performance and the fabrication reliability. In addition, the extended analysis is qualitatively explored using the dispersion relation to clarify the effects of LSP modes.

This paper is organized as follows. In Section 2, a numerical model based on the rigorous coupled-wave analysis (RCWA) is described. Results of obtaining optimal nanowire structure based on various design parameters, such that it maximizes localized surface plasmon resonance, are presented in Section 3. Qualitative analysis of the sensitivity enhancement is discussed based on the dispersion relation between an incident photon and an LSP in Section 4, which is followed by concluding remarks in Section 5.

2. Numerical model

For numerical analysis, RCWA has been employed to obtain optical characteristics of a periodic structure of gold nanowires on a smooth gold film. For RCWA, the complex dielectric function of a metallic nanowire grating is written as a Fourier series expansion

$$\varepsilon(x, z) = \varepsilon(x + \Lambda, z) = \sum_m \varepsilon_m(z) \exp(jmK_G x), \quad (1)$$

where Λ is the grating period, ε_m the Fourier component of the grating dielectric function, and $K_G = 2\pi/\Lambda$ is the grating vector. The coordinates in Eq. (1) are depicted in Fig. 1. The light source is assumed to be a unit-amplitude monochromatic plane wave with wavelength λ and an incidence angle θ with the z-axis. An electric or a magnetic field inside a grating region with a complex dielectric function is determined by solving two wave equations,

$$\nabla^2 \vec{E} + \nabla \left(\vec{E} \cdot \frac{\nabla \varepsilon}{\varepsilon} \right) + k^2 \varepsilon(x, z) \vec{E} = 0, \quad (2)$$

$$\nabla^2 \vec{H} + \frac{\nabla \varepsilon}{\varepsilon} \times \nabla \times \vec{H} + k^2 \varepsilon(x, z) \vec{H} = 0, \quad (3)$$

where $\vec{E}$ and $\vec{H}$ are the electric and magnetic field intensity, respectively. k ($=2\pi/\lambda$) is the wave number in the free space. For a particular polarization component of incident light, Eq. (2) or (3) can be simplified, leading to RCWA expressed as an infinite set of coupled-wave equations where the electric or magnetic field is expanded in terms of space-harmonic components with variable amplitudes in the z-direction [25,26]. The space-harmonic amplitudes are then solved for the coefficient matrix using eigenvalues and eigenvectors of the differential equation. While the total coefficient matrix is an infinite one, calculation results can be obtained in practice to an arbitrary level of accuracy with a truncated matrix. Each space-harmonic component inside a metallic grating is phase-matched to a diffraction order. Because the tangential components of electric and magnetic fields must be continuous at boundaries of a grating, the field of each diffraction order outside a grating is related to the corresponding space-harmonic inside a grating. Note that since the field is more rapidly varying in short distances of a nanostructure with a size smaller than 100 nm, more space-harmonic components are needed to attain the convergence and to improve the accuracy in calculation.

The RCWA has been successfully applied to explaining experimental results that involve nanostructures [27–29]. It should be noted that our RCWA routine was found to corroborate earlier studies using nanowires that range a few tens of nanometers in size [30]. For instance, Schider et al. found, by fabricating one-dimensional silver nanowires ($\Lambda = 2250$ nm) with a cross-section of 83 nm in width and 25 nm in height on a thin layer of indium tin oxide and a fused quartz substrate, that the optical response of regularly patterned nanowires strongly depends on the polarization of the incident light [31]. The extinction spectra produced by RCWA, shown in Fig. 2, are in excellent agreement with experimentally obtained results; for TM polarization, the extinction maximum is located near 500 nm and the full width at half maximum is approximately 120 nm. On the other hand, for TE polarization, no resonance is found as was empirically observed. The extinction grows slightly with increased wavelength due to the absorption of silver. Note that the position of an extinction peak indicates the resonance wavelength while the spectral width exhibits the damping of plasmon resonance induced by nanowires.

In addition, optical properties of two-dimensional metallic nanoparticles on a transparent dielectric substrate were also

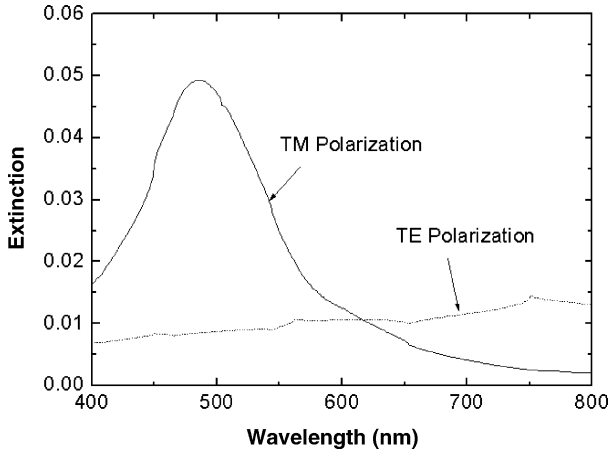

Fig. 2. Calculated extinction spectra of silver nanowires for TM and TE polarizations. The plasmon resonance is found for TM polarization, but not for TE polarization. The optical extinction is defined as $\log(T_0/T)$, where T_0 and T are the magnitudes of the optical transmission through the bare substrate and the nanowire sample deposited on a substrate.

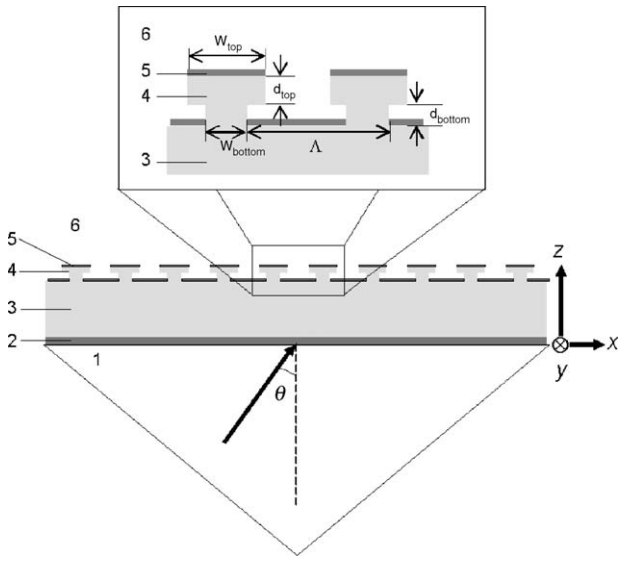

Fig. 3. Schematic diagram of a nanowire-mediated localized SPR biosensor with gold nanowires of a T-profile on a gold film. The illumination at a fixed wavelength 633 nm is incident at an angle θ in the xz-plane. Layers 1, 2, 3, 4, 5, and 6 represent a BK7 glass prism, a layer of chromium, a gold film, one-dimensional gold nanowires, target analytes, and air, respectively. The thickness of each layer is 2 nm (d_2), 40 nm (d_3), 20 nm (d_4), and 1 nm (d_5).

reproduced with RCWA [30,32]. While detailed results are not shown here, the optical extinction of Ag nanoparticles at different aspect ratios was calculated by modeling as Ag nanowires for TM and TE polarizations. Since two-dimensional arrays, so called cross gratings, can be represented as a structural sum of two gratings that cross at right angles (one in the lateral direction and the other longitudinally), approximation of two-dimensional nanoparticles as one-dimensional nanowires is supported in the case that there is no coupling between given polarized light and the grating when the grating vector is perpendicular to the polarization direction. The spectral characteristics for TM polarization showed that a change in aspect ratio leads to a distinguishable increase of peak positions, while the extinction peak on the long-wavelength side disappeared for TE polarization. The experimentally observed general trends have agreed very well with the numerical results, which confirms that RCWA provides a useful tool to analyze the optical properties of nanowires.

In the current study, RCWA has been employed to investigate a nanowire-mediated localized SPR biosensor with a schematic diagram shown in Fig. 3. One-dimensional gold nanowires with period Λ oriented along the y-axis are regularly patterned on a gold film that supports SPP modes. A 2-nm thick layer of chromium attaches the gold film to a prism. Binding analytes are modeled as a 1-nm thick self-assembled monolayer (SAM) of refractive index 1.526, which covers both gold nanowires and a gold film. The thickness of the gold film is 40 nm for both conventional and nanowire-mediated localized SPR configurations. Since a SAM layer is extremely thin compared with the wavelength of incident light, the absorption can be neglected so that the layer is essentially a dielectric [15]. A TM-polarized light of $\lambda = 633$ nm is incident on a side of the prism and the incidence angle is scanned with an angular resolution $\Delta\theta = 0.01^\circ$. The dielectric function of a BK7 glass prism and of chromium and gold layers was determined, respectively, as 1.515, $3.48 + 4.36i$, and $0.18 + 3.0i$ at $\lambda = 633$ nm [33].

Based on the reports that nanostructures ranging from 20 to 50 nm in size produce the strongest and sharpest SPR sensitivity enhancement [14,15,17], gold nanowires considered in this study are also sized in this range. In particular, one-dimensional nanowires with a T-, an inverse T-, or a rectangular profile are under consideration for the analysis using a schematic shown in Fig. 3, where w_{top} (w_{bottom}) denoting the width of the nanowire top (bottom) is either 20 or 40 nm. The nanowire depth d_4 ($= d_{top} + d_{bottom}$) is fixed at 20 nm. For convenience, a geometry factor (GF) of nanowires is introduced as d_{top}/d_4 if $w_{top} > w_{bottom}$ for a T-profile and d_{bottom}/d_4 if $w_{top} < w_{bottom}$ for an inverse T-profile. A GF is defined to be 0 if $w_{top} = w_{bottom} = 20$ nm, and 1 if $w_{top} = w_{bottom} = 40$ nm for a rectangular profile. Consequently, T- and inverse T-profiles have an equal volume of nanowires if the GF is the same.

3. Results

To represent the impact of nanowires on the sensitivity enhancement quantitatively, a sensitivity enhancement factor (SEF) is introduced as

$$\mathrm{SEF} = \frac{|\theta_{\mathrm{NWSPR}}(\text{with analytes}) - \theta_{\mathrm{NWSPR}}(\text{without analytes})|}{\Delta\theta_{\mathrm{SPR}}}, \tag{4}$$

where the subscripts NWSPR and SPR represent the plasmon resonance angles with and without analytes of a nanowire-mediated localized SPR configuration and a conventional SPR scheme [24].

Fig. 4 shows the calculated reflectance characteristics of a conventional SPR configuration. The resonance angles with and without bound analytes are 45.29° and 45.12°; thus the resonance shift $\Delta\theta_{\mathrm{SPR}} = 0.17^\circ$. Since SPR curves are highly asymmetric, the SPR CAW is defined as the angle difference between

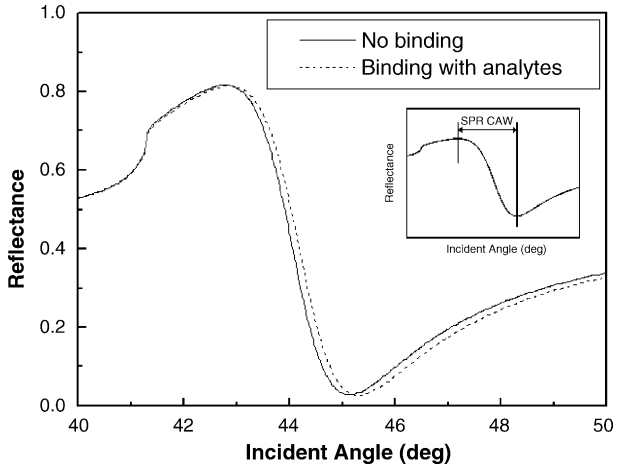

Fig. 4. SPR curves of a conventional SPR biosensor shown in Fig. 1. The thickness of each layer is 2 nm (chromium), 40 nm (gold), and 1 nm (target analytes). The solid and dotted curves represent without binding and with binding to analytes. The resonance angles are 45.12° and 45.29°, respectively. The inset describes the definition of the SPR CAW as the angular difference between reflectance minimum and maximum.

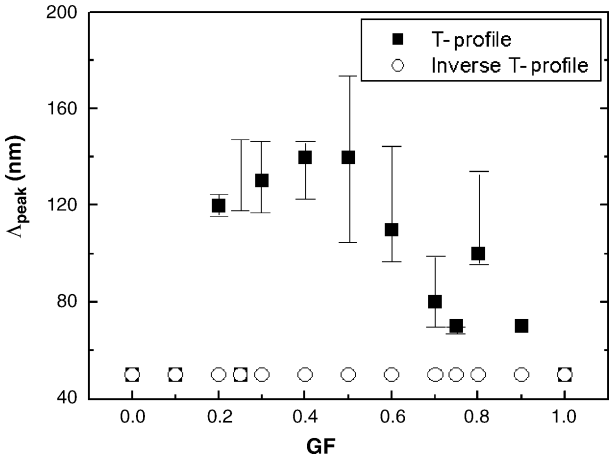

Fig. 6. Nanowire period, Λ_{peak}, with GF when the SEF is the highest for nanowires of a T-profile (■) and an inverse T-profiles (◯). The vertical line shown of the T-profiles indicates the range of nanowire periods in which the SEF exceeds a given SEF threshold. The threshold is set to be 20, the maximum SEF obtained from an inverse T-profile.

reflectance minimum and maximum as presented in the inset of Fig. 4. The SPR CAW and MRR are obtained as 2.40° and 0.03 for a conventional SPR configuration.

Using Eq. (4), peak SEFs calculated for T- and inverse T-profiles and presented in Fig. 5 show that a T-profile generally exhibits a larger SEF than an inverse T-profile. The highest SEF obtained of a T-profile is 47.35 at GF = 0.25, while that of an inverse T-profile is 19.29 when the GF = 0.9. For a T-profile, both dominantly excited LSP modes and the structure effect that incurs relatively small interference between substrate and nanowires lead to great improvement of sensitivity [24]. For an inverse T-profile, however, LSPs are not resonantly excited as the strong interaction with a substrate results in damping of LSP modes.

In Fig. 6 that represents the nanowire period at the peak SEF as the GF varies, the highest SEF for an inverse T-profile is obtained at $\Lambda = 50$ nm, i.e., $\Lambda_{peak} = 50$ nm, with all values of GF. On the other hand, for a T-profile, Λ_{peak} varies from 50 to 140 nm. From Figs. 5 and 6, a nanowire-mediated localized SPR biosensor with a T-profile generally results in larger sensitivity enhancement, particularly at a longer nanowire period. This, in turn, implies that nanowires of a T-profile, since they achieve better performance at a longer period, are relatively easy to fabricate. The vertical line of a T-profile in Fig. 6 indicates the range of nanowire periods, $\Delta\Lambda$, in which the SEF exceeds a given threshold. The range $\Delta\Lambda$ can measure performance reliability and robustness to fabrication errors in implementing nanowires and thus a wide range is desired. The SEF threshold for a T-profile is set to be 20, since it is the maximum SEF of an inverse T-profile (see Fig. 5). Thus, the SEF at nanowire periods that are included in the vertical line is to be higher than that of an inverse T-profile and the threshold. A nanowire structure of GF = 0.5 has the widest range of nanowire periods (Λ = 105–172 nm, i.e., the width of the range $\Delta\Lambda$ = 67 nm) at which a SEF exceeds the threshold. At GF = 0.6 and 0.8, $\Delta\Lambda$ is also significant, larger than 30 nm. Note that at GF = 0.25, the vertical line is shown as ranging from 109 to 137 nm while Λ_{peak} = 50 nm. This implies that $\Delta\Lambda$ in the vicinity of Λ_{peak} is extremely narrow and the SEF can still exceed the threshold at a longer nanowire period far from Λ_{peak}. It is clear from Figs. 5 and 6 that nanowires of a T-profile exhibits better characteristics than those of an inverse T-profile, in terms of the peak SEF, Λ_{peak}, and $\Delta\Lambda$.

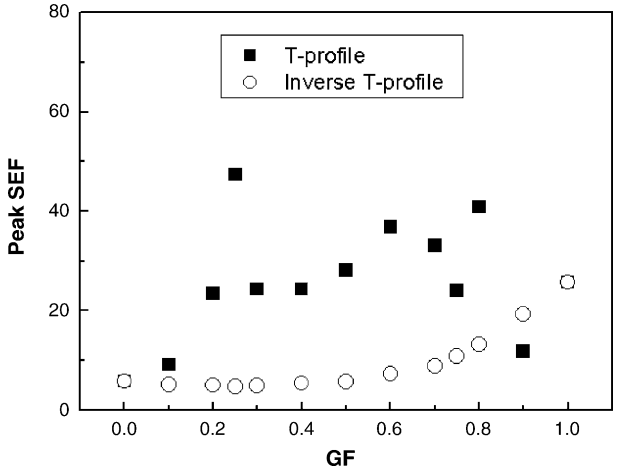

Fig. 5. Peak SEF with GF for nanowires of a T-profile (■) and an inverse T-profile (◯). GF varies from 0 to 1.

For practical applications of a nanowire-mediated localized SPR biosensor, structural optimization based on the peak SEF, Λ_{peak}, and $\Delta\Lambda$ may not be sufficient. For good performance, nanowires with a narrow CAW and a small MRR are desired, because with a highly broad CAW and a shallow MRR, it becomes quite difficult to accurately detect the resonance position and to analyze precisely the effect of binding events on a SPR structure. For this reason, in the design process, other practically important SPR properties such as CAW and MRR were also counted in besides the angular shift of resonance.

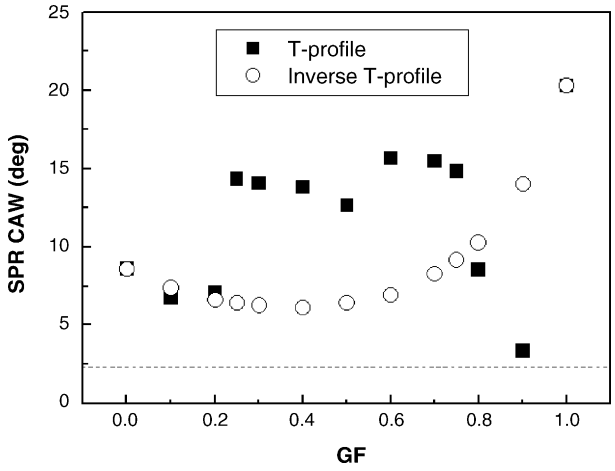

Fig. 7. The SPR CAW with GF for nanowires of a T-profile (■) and an inverse T-profile (◯). The dotted line indicates the SPR CAW of a conventional SPR scheme in Fig. 4.

Broader SPR CAW implies the resonance condition more loosely met due to the presence of nanowires since a wide SPR CAW involves LSPs excited around the resonance with diverse momentum matching conditions. As observed in Figs. 7 and 8, the CAW and the MRR are largely increased as LSP modes in nanowires are excited. Generally, the SPR CAW of a T-profile is larger than that of an inverse T-profile as shown in Fig. 7. The contrast between the two profiles is starker in the MRR characteristic in Fig. 8. The prominent difference stems from nanowire-induced perturbation in the dispersion relation of SPR as discussed in the subsequent section in more detail. In Fig. 8, since LSP modes are in resonance, nanowires of a T-profile show an increased MRR. However, for an SPP-dominated inverse T-profile, the MRR is comparable to that of a conventional SPR configuration. Our numerical results show that in general, a T-profile brings about larger damping of SPP modes and more resonantly excited LSP modes than an inverse T-profile. Thus, use of a T-profile improves the sensitivity of nanowire-mediated localized SPR biosensors more efficiently.

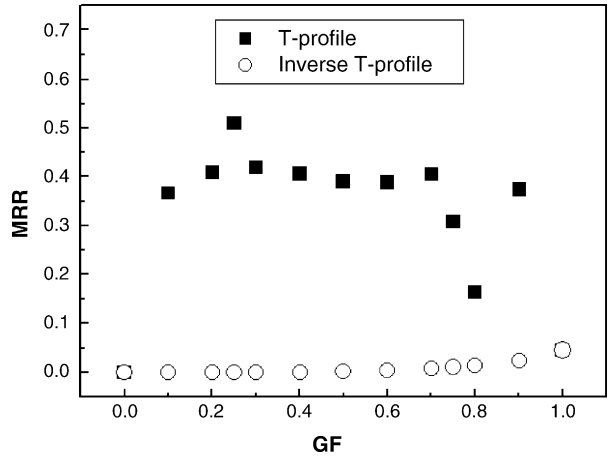

Fig. 8. The MRR with GF for nanowires of a T-profile (■) and an inverse T-profile (◯).

Considering that a T-profile shows a larger SEF than an inverse T-profile and also that small values of CAW and MRR are obtained around GF = 0.8 for a T-profile, optimized nanowires are a T-profile at GF = 0.8. From Figs. 5 and 6, these nanowires achieve the peak SEF = 40.91 at $\Lambda_{peak} = 100$ nm. The $\Delta\Lambda$ is 32 nm (from 96 to 128 nm), which is large enough not to be sensitive to fabrication errors in nanowire period. At this GF, the CAW is relatively narrow while the MRR is the smallest compared with those obtained at other GFs of a T-profile.

4. Discussion

Compared with a conventional SPR scheme, the existence of nanostructures near the metallic film leads to significant perturbation of the dispersion relation of SPP modes. In particular, when the excitation of LSP modes are dominant, large SPP damping is observed as it makes SPR curves broader and shallower and also induces the resonance at higher angle.

Fig. 9 presents the resonance angles of a nanowire-mediated localized SPR biosensor with different profiles, as GF varies from 0 to 1. Calculation results show that the resonance angle generally changes to a larger value due to the presence of nanowires, compared with the characteristics of a conventional SPR scheme shown as the dotted line in Fig. 9. Especially, when a GF is in the range of 0.25–0.75, the shift in a T-profile is larger than in an inverse T-profile. In the case of GF = 0.9 for a T-profile, the resonance angle is nearly close to that of a conventional SPR scheme. It is expected that the influence of LSPs at GF = 0.9 of a T-profile should be insignificant with limited sensitivity enhancement. The resonance angle shift shown in Fig. 9 is similar in appearance to the broadening of the SPR CAW observed in Fig. 7, which is due to the damping of SPP modes as the effect of LSPs excited in nanowires becomes more dominant than SPP modes and results in the enhanced sensitivity. The disparity between T- and inverse T-profiles is more evident in the GF range of 0.25–0.75. At other values of GF, the SPR CAW of a T-profile with smaller resonance angle becomes comparable

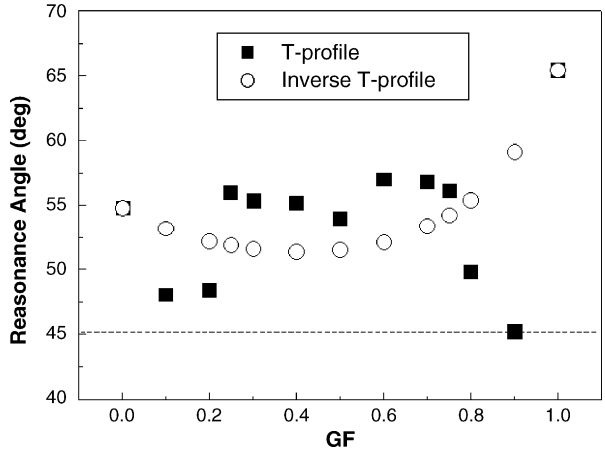

Fig. 9. Resonance angles for nanowires of a T-profile (■) and an inverse T-profile (◯). The incident light is TM-polarized with a fixed wavelength of 633 nm. The dotted line represents the resonance angle of a conventional SPR biosensor shown in Fig. 4.

to that of an inverse T-profile. These results are attributed to two processes; absorption damping and localized coupling between SPPs and LSPs. In the case of an inverse T-profile, though excited LSPs may induce minor changes in SPP features, the SPP modes still dominate so that the LSPs do not resonantly affect the SPR with a limited impact of nanowires.

Impacts of nanowire profiles on the SPR characteristics can also be studied using the dispersion relation. Across the interface between a metal film and a surrounding dielectric medium, the wave vector, k_{spp}, is continuous for momentum matching, so that the dispersion relation can be written as [6,23]

$$k_{spp} = \frac{w}{c}\left(\frac{\varepsilon_M \varepsilon_D}{\varepsilon_M + \varepsilon_D}\right)^{1/2}, \quad (5)$$

where w and c denote the angular frequency and the speed of light in the free space. And $\varepsilon_M\,(=\varepsilon'_M + i\varepsilon''_M)$ and ε_D are the complex dielectric functions of a metal film and a dielectric medium. In the case of $\varepsilon''_M < \varepsilon'_M$, the complex term k_{spp} is taken as

$$Re(k_{spp}) = \frac{w}{c}\left(\frac{\varepsilon'_M \varepsilon_D}{\varepsilon'_M + \varepsilon_D}\right)^{1/2}, \quad (6)$$

$$Im(k_{spp}) = \frac{w}{c}\left(\frac{\varepsilon'_M \varepsilon_D}{\varepsilon'_M + \varepsilon_D}\right)^{3/2} \frac{\varepsilon''_M}{2(\varepsilon'_M)^2}. \quad (7)$$

As is well known, the resonance angle and the SPR CAW are correlated to the real and imaginary part of k_{spp}, respectively [16], i.e., a large real part induces a large shift of resonance angle and a large imaginary part similarly leads to a large SPR CAW. Also, a large CAW implies large damping of SPP modes, which in turn implies the dominant influence of LSP modes.

The different performance between T- and inverse T-profiles can be described more clearly in view of the SPR CAW as shown in Fig. 7. In general, the absorption coefficient (κ_M) of noble metal is much larger than the refractive index (n_M). If we assume that $\kappa_M^2 \gg n_M^2 \approx 0$ at $\lambda = 633$ nm, the imaginary part of k_{spp} is related to n_M and κ_M by

$$Im(k_{spp}) = \frac{w n_D^3}{c}\left(\frac{\kappa_M^2}{\kappa_M^2 - n_D^2}\right)^{3/2} \frac{n_M}{\kappa_M^3}, \quad (8)$$

where n_D is the refractive index of a dielectric medium. Eq. (8) shows that the SPR CAW is more dominantly influenced by the large absorption coefficient of the gold film than refractive index and other parameters.

In particular, the imaginary part of k_{spp} is related to the absorption damping effect induced by the structural difference between the two profiles. Since nanowires of an inverse T-profile have a larger interface with the gold film than those of a T-profile, the effective absorption of the gold film that supports nanowires of an inverse T-profile becomes also larger. From Eq. (8), the larger the absorption coefficient is, the smaller the imaginary part of k_{spp}. This implies that the SPR CAW is not largely broad and the SPP modes are still influential. On the other hand, nanowires of a T-profile with a narrow contact area to a gold film exhibit smaller effective absorption than those of an inverse T-profile. Thus, the gold film with nanowires of a T-profile exhibits a larger imaginary component, resulting in a larger SPR CAW. Moreover, as nanowires attached to the gold film excite LSPs, the LSPs interact with the SPPs that are formed on the surface of the gold film. Larger coupling interaction between LSPs and SPPs for an inverse T-profile than for a T-profile results in greater interference and damping of excited LSPs [24].

5. Conclusions

We have studied the impact of nanowires on the sensitivity enhancement of SPR biosensors using RCWA. Compared with a conventional SPR scheme, nanowires built on a gold film lead to significant deformation of the dispersion relation of SPP modes. Especially when LSP modes couple resonantly, broad SPR CAW and shallow MRR as well as a large shift of the resonance angle can be observed due to absorptive damping and localized coupling. Also, nanowires of a T-profile are found to present higher sensitivity enhancement than those of an inverse T-profile. The impact of the nanowire profile is investigated qualitatively using the dispersion relation of gold–dielectric interface.

Also, optimal design parameters of nanowires are determined based on quantitative metrics that measure the sensor performance and the fabrication reliability. Optimal nanowires are a T-profile with a GF = 0.8 ($w_{top} = 40$ nm, $w_{bottom} = 20$ nm, $d_{top} = 16$ nm and $d_{bottom} = 4$ nm). This geometry results in significantly enhanced sensitivity over 40 times larger than that of a conventional SPR biosensor. In addition, a relatively large width of nanowire periods, $\Delta\Lambda$, in which the SEF exceeds a pre-set threshold, was determined to be more than 30 nm. Our study on a nanowire-mediated localized SPR biosensor offers physical insights to understanding the sensitivity enhancement mechanism and demonstrates the potential for significant improvement in the sensitivity using the designed nanowire structure.

Acknowledgements

This work was supported by the SRC/ERC program of MOST/KOSEF (R11-2000-075-01001-1). D. Kim acknowledges the support by KOSEF through National Core Research Center for Nanomedical Technology (R15-2004-024-00000-0).

References

[1] B. Rothenhäusler, W. Knoll, Surface-plasmon microscopy, Nature 332 (1988) 615–617.
[2] C. Nylanderm, B. Liedberg, T. Lind, Gas detection by means of surface plasmon resonance, Sens. Actuators 3 (1982–1983) 79–88.
[3] K. Matsubara, S. Kawata, S. Minami, Optical chemical sensor based on surface plasmon measurement, Appl. Opt. 27 (1988) 1160–1163.
[4] S. Löfås, B. Johnson, A novel hydrogel matrix on gold surfaces in surface plasmon resonance sensors for fast and efficient covalent immobilization of ligands, J. Chem. Soc. Chem. Commun. 21 (1990) 1526–1528.
[5] J. Homola, S.S. Yee, G. Gauglitz, Surface plasmon resonance sensors: review, Sens. Actuators B 54 (1999) 3–15.
[6] H. Raether, Surface Plasmon on Smooth and Rough Surfaces and on Gratings, Springer–Verlag, Berlin, 1988.

[7] E. Kretschmann, Die Bestimmung optischer Konstanten von Metallen durch Anregung von Oberflächen-plasmaschwingungen, Z. Phys. 241 (1971) 313–324.
[8] M. Malmqvist, Surface plasmon resonance for detection and measurements of antibody–antigen affinity and kinetics, Curr. Opin. Immunol. 5 (1993) 282–286.
[9] T. Akimoto, S. Sasaki, K. Ikebukuro, I. Karube, Effect of incident angle of light on sensitivity and detection limit for layers of antibody with surface plasmon resonance spectroscopy, Biosens. Bioelectron. 15 (2000) 355–362.
[10] B.P. Nelson, T.E. Grimsrud, M.R. Liles, R.M. Goodman, R.M. Corn, Surface plasmon resonance imaging measurements of DNA and RNA hybridization adsorption onto DNA microarrays, Anal. Chem. 73 (2001) 1–7.
[11] R.J. Leatherbarrow, P.R. Edwards, Analysis of molecular recognition using optical biosensors, Curr. Opin. Chem. Biol. 3 (1999) 544–547.
[12] B. Johnsson, S. Löfås, G. Lindquist, Immobilization of proteins to a carboxymethyldextran-modified gold surface for biospecific interaction analysis in surface plasmon resonance sensors, Anal. Biochem. 198 (1991) 268–277.
[13] B. Liedberg, C. Nylander, I. Lundstrom, Biosensing with surface plasmon resonance—how it all started, Biosens. Bioelectron. 10 (1995) 1–4.
[14] L.A. Lyon, M.D. Musick, M.J. Natan, Colloidal Au-enhanced surface plasmon resonance immunosensing, Anal. Chem. 70 (1998) 5177–5183.
[15] E. Hutter, S. Cha, J.-F. Liu, J. Park, J. Yi, J.H. Fendler, D. Roy, Role of substrate metal in gold nanoparticle enhanced surface plasmon resonance imaging, J. Phys. Chem. B 105 (2001) 8–12.
[16] T. Kume, N. Nakagawa, S. Hayashi, K. Yamamoto, Interaction between localized and propagating surface plasmons: Ag fine particles on Al surface, Solid State Commun. 93 (1995) 171–175.
[17] L.A. Lyon, D.J. Pena, M.J. Natan, Surface plasmon resonance of Au colloid-modified Au films: particle size dependence, J. Phys. Chem. B 103 (1999) 5826–5831.
[18] L. He, M.D. Musick, S.R. Nicewarner, F.G. Salinas, S.J. Benkovic, M.J. Natan, C.D. Keating, Colloidal Au-enhanced surface plasmon resonance for ultrasensitive detection of DNA hybridization, J. Am. Chem. Soc. 122 (2000) 9071–9077.
[19] M.D. Malinsky, K.L. Kelly, G.C. Schatz, R.P. Van Duyne, Chain length dependence and sensing capabilities of the localized surface plasmon resonance of silver nanoparticles chemically modified with alkanethiol self-assembled monolayers, J. Am. Chem. Soc. 123 (2001) 1471–1482.
[20] A.J. Haes, R.P. Van Duyne, A nanoscale optical biosensor: sensitivity and selectivity of an approach based on the localized surface plasmon resonance spectroscopy of triangular silver nanoparticles, J. Am. Chem. Soc. 124 (2002) 10596–10604.
[21] Z. Salamon, M.F. Brown, G. Tollin, Plasmon resonance spectroscopy: probing molecular interactions within membranes, Trends Biochem. Sci. 24 (1999) 213–219.
[22] D. Roy, Optical characterization of multi-layer thin films using the surface plasmon resonance method: a six-phase model based on the Kretschmann formalism, Opt. Commun. 200 (2001) 119–130.
[23] I. Pockrand, Surface plasma oscillations at silver surfaces with thin transparent and absorbing coatings, Surf. Sci. 72 (1978) 577–588.
[24] K.M. Byun, S.J. Kim, D. Kim, Design study of highly sensitive nanowire-enhanced surface plasmon resonance biosensors using rigorous coupled wave analysis, Opt. Express 13 (2005) 3737–3742, http://www.opticsexpress.org/abstract.cfm?URI=OPEX-13-10-3737.
[25] M.G. Moharam, T.K. Gaylord, Diffraction analysis of dielectric surface-relief gratings, J. Opt. Soc. Am. 72 (1982) 1385–1392.
[26] M.G. Moharam, T.K. Gaylord, Rigorous coupled-wave analysis of metallic surface-relief gratings, J. Opt. Soc. Am. A 3 (1986) 1780–1787.
[27] Y. Kanamori, K. Hane, H. Sai, H. Yugami, 100 nm period silicon antireflection structures fabricated using a porous alumina membrane mask, Appl. Phys. 78 (2001) 142–143.
[28] T.R. Jensen, L. Kelley, A. Lazarides, G.C. Schatz, Electrodynamics of noble metal nanoparticles and nanoparticle clusters, J. Cluster Sci. 10 (1999) 295–317.
[29] S. Park, G. Lee, S.H. Song, C.H. Oh, P.S. Kim, Resonant coupling of surface plasmons to radiation modes by use of dielectric gratings, Opt. Lett. 28 (2003) 1870–1872.
[30] K.M. Byun, D. Kim, S.J. Kim, Investigation of the sensitivity enhancement of nanoparticle-based surface plasmon resonance biosensors using rigorous coupled-wave analysis, in: T. Vo-Dinh, J.R. Lakowicz, Z.K. Gryczynski (Eds.), Plasmonics in Biology and Medicine II, Proceedings of SPIE 5703, 2005, pp. 61–70.
[31] G. Schider, J.R. Krenn, W. Gotschy, B. Lamprecht, H. Ditlbacher, A. Leitner, F.R. Aussenegg, Optical properties of Ag and Au nanowire gratings, J. Appl. Phys. 90 (2001) 3825–3830.
[32] W. Gotschy, K. Vonmetz, A. Leitner, F.R. Aussenegg, Optical dichroism of lithographically designed silver nanoparticle films, Opt. Lett. 21 (1996) 1099–1101.
[33] E.D. Palik, Handbook of Optical Constants of Solids, Academic Press, Orlando, FL, 1985.

Biographies

Kyung Min Byun was born in 1977 and he received the master's degree in electrical engineering at Seoul National University, Seoul, South Korea in 2002. He is currently in the PhD program at the same university, presently working on SPR biosensors based on nanostructures. His current interests include the theoretical and experimental study of extremely sensitive SPR biosensors and the implementation and characterization of nanostructure-based localized SPR.

Donghyun Kim received the BS and MS degrees in electronics engineering, respectively, in 1993 and 1995 from Seoul National University and the PhD degree in electrical engineering from Massachusetts Institute of Technology, Cambridge, MA, USA in 2001. He had been with Corning Inc., Corning, NY, USA and with Cornell University, Ithaca, NY, USA before he joined Yonsei University in 2004. His current research interests are focused on biomedical applications of opto-electonics including surface plasmon resonance, live-cell imaging, and in vivo optical imaging.

Sung June Kim received the BS degree in electronics engineering from Seoul National University in 1978 and the MS and PhD degrees from Cornell University, Ithaca, NY, USA in 1981 and 1983, respectively. He had been with the AT&T Bell Laboratories as a member of the technical staff from 1983 to 1989, where he had worked on VLSI design and technologies, and InP based opto-electronic IC technologies. In 1989, he joined Seoul National University as a professor. In 2000, he started the Nano-Bioelectronics and Systems Research Center as director, which is an ERC sponsored by the Korean Science and Engineering Foundation (KOSEF). His research activity is devoted to the design and fabrication of neural prostheses systems, development of nano and micro technologies for neural applications, and design of ASIC for neural signal processing.